Cell. Mol. Life Sci. (2009) 66:2773–2787
DOI 10.1007/s00018-009-0079-2

Cellular and Molecular Life Sciences

RESEARCH ARTICLE

Oxidative stress triggers neuronal caspase-independent death: Endonuclease G involvement in programmed cell death-type III

Gavin C. Higgins · Philip M. Beart · Phillip Nagley

Received: 30 April 2009 / Revised: 26 May 2009 / Accepted: 17 June 2009 / Published online: 7 July 2009

Abstract To characterize neuronal death, primary cortical neurons (C57/Black 6 J mice) were exposed to hydrogen peroxide (H_2O_2) and staurosporine. Both caused cell shrinkage, nuclear condensation, DNA fragmentation and loss of plasma membrane integrity. Neither treatment induced caspase-7 activity, but caspase-3 was activated by staurosporine but not H_2O_2. Each treatment caused redistribution from mitochondria of both endonuclease G (Endo G) and cytochrome *c*. Neurons knocked down for Endo G expression using siRNA showed reduction in both nuclear condensation and DNA fragmentation after treatment with H_2O_2, but not staurosporine. Endo G suppression protected cells against H_2O_2-induced cell death, while staurosporine-induced death was merely delayed. We conclude that staurosporine induces apoptosis in these neurons, but severe oxidative stress leads to Endo G-dependent death, in the absence of caspase activation (programmed cell death-type III). Therefore, oxidative stress triggers in neurons a form of necrosis that is a systematic cellular response subject to molecular regulation.

Keywords Programmed cell death · Apoptosis · Necrosis · Oxidative stress · Neurons · Caspases · Endonuclease G · Mitochondria

Introduction

Oxidative stress is a feature of many neurodegenerative disorders and occurs chronically in diseases such as Parkinson's and Alzheimer's disease [reviewed in 1, 2]. In a more acute setting, oxidative stress is a significant pathogenic factor following cerebral ischemic reperfusion after stroke [reviewed in 3]. In many stroke models the generation of reactive oxygen species (ROS) is elevated following cerebral ischemia [4–8]. The severity of the cerebral ischemia and the subsequent reperfusion are considered to determine the particular cell death pathways triggered within injured neurons. Tissue injury in the stroke-affected brain has traditionally been considered to involve either necrosis or apoptosis. Thus, at the core or center of infarction, the most severe damage to neurons occurs, involving massive necrosis. Such death involves failure of ionic gradients across the plasma membrane (PM) and within cells associated with neuronal depolarization in the face of anoxia and reduced use of glucose by cells. At the boundary of the core and penumbra, excitotoxicity due to excess glutamate occurs; here the cells have adequate glucose supply, but die from ionic imbalances, significantly calcium overload [9]. Mechanisms of death by excitotoxicity have been appraised in substantial detail [10–13]. Apoptosis was initially regarded the predominant cell death process in the penumbra, in the face of multiple cellular insults including neurotransmitter overload, excess of K^+ ions, as well as oxidative stress [reviewed in 9]. However, a broader spectrum of death responses, perhaps

Electronic supplementary material The online version of this article (doi:10.1007/s00018-009-0079-2) contains supplementary material, which is available to authorized users.

G. C. Higgins · P. Nagley (✉)
Department of Biochemistry and Molecular Biology, Monash University, Building 13D, Clayton Campus, Clayton, VIC 3800, Australia
e-mail: phillip.nagley@med.monash.edu.au

P. M. Beart
Florey Neuroscience Institutes and Department of Pharmacology, University of Melbourne, Parkville, VIC, Australia

representing a continuum of possible death pathways ranging across apoptosis to necrosis [14–17] as well as autophagy and other mechanisms [18], is now considered to encompass the neuronal responses to the range of insults in the penumbra.

Therefore, cell death, once succinctly defined as either apoptotic (programmed with caspase activation) or necrotic (non-programmed without caspase involvement), can no longer be discriminated by such simple classification. Currently, programmed cell death (PCD) pathways are subdivided into three major types. These encompass PCD-type I (apoptosis), PCD-type II (autophagic cell death) and PCD-type III (programmed necrosis) [19]. PCD-type III therefore manifests features of necrosis by definition; however, it differs from unregulated necrosis in that PCD-type III can be regulated and can be inhibited like other forms of PCD. Necrosis is marked by cell swelling, gross PM rupture and little or no involvement of caspases [19].

There are several reports of cultured neuronal cells undergoing PCD-type III under various stimuli. These include descriptions of caspase-independent apoptosis in primary cerebellar granule cells and cortical neurons exposed to excitotoxic analogues, (e.g., AMPA, kainate) [10, 11, 13, 20]. However, features of neuronal death that warrant more substantial investigation involve the response to oxidative stress, particularly the role of caspases, and the possibility that PCD-type III is an outcome of neurons exposed to severe oxidative stress, as may occur in cerebral ischemia-reperfusion injury.

In this study we set out to determine whether primary murine cortical neurons undergo PCD-type III, triggered by oxidative insult. Endonuclease G (Endo G) was studied as a significant mediator of cell death in the absence of caspase activation [21]. There are two mitochondrial proteins, apoptosis-inducing factor (AIF) and Endo G, which drive apoptotic nuclear DNA fragmentation in the absence of caspases [13, 20–22]. However, AIF seems less useful than Endo G where oxidative stress is the insult because of the known antioxidant properties of AIF that underlie its involvement as a protector of cells against oxidative stress on the one hand and a death-mediating protein on the other [23, 24]; these dual roles confer ambiguity on the interpretation of experimental data. During death signaling, Endo G has been shown to translocate from the mitochondrial intermembrane space (IMS) to the nucleus to participate in non-specific DNA fragmentation, similar to its pro-death counterpart AIF [21, 22]. Moreover, the characterization of primary neuron dependency on Endo G in PCD signaling during oxidative insult has not been thoroughly undertaken until now.

We used primary embryonic cortical neurons from C57/Black 6 J mice, a murine strain frequently used as background for many genetic animal modifications [25, 26]. Hydrogen peroxide (H_2O_2) was used as the death-inducing oxidative insult, alongside staurosporine (STS), a widely used inducer of apoptosis [27] to help differentiate between PCD-type I and other PCD pathways. Analysis of caspase-dependent cell death together with knockdown of Endo G levels in cultured neurons revealed that, whereas STS induces apoptosis, H_2O_2 treatment leads to caspase-independent PCD-type III. Moreover, our data revealed a specific role for Endo G as a central component PCD-type III under oxidative insult.

Materials and methods

Cell culture

Primary cultures of murine neocortical neurons were established from embryonic day 15 C57/Black 6 J mice, as previously described [10, 28]. Under these conditions the cultures were essentially purely neuronal and contained <5% astrocytes [10, 28]. All experimentation received institutional ethical approval and was undertaken according to the Guidelines of the NH&MRC (Australia).

Short interfering RNA (siRNA) transfections

Endo G siRNAs (product name: Mm_Endog_4_HP Validated siRNA), AIF siRNA (product name: Mm_Pdcd8_3_HP Validated siRNA) and negative control siRNA were purchased from Qiagen (Germantown, MD, USA). Transfection of mouse primary cortical neurons with siRNA was carried out by using HiPerFect transfection reagent (Qiagen, Doncaster, Vic, Australia) according to the protocols provided by the manufacturer. Under these conditions, typically 50–70% of neuronal cells were transfected by control siRNA. Briefly, neurons were transfected in 6-well (for immunoblotting; 2.5×10^6 cells) or 24-well plates (on glass coverslips for microscopic imaging; 0.5×10^6 of cells) on day 3 in vitro. Neurons were subsequently left in culture until day 7 in vitro, where treatments with STS and H_2O_2 were performed.

Drug exposure

Guided by our previous work [10, 11], neuronal cultures were exposed to either 50 μmol/l H_2O_2 [30% (w/v), Merck, Melbourne, Vic, Australia] or 200 nmol/l STS (Sigma-Aldrich, Castle Hill, NSW, Australia) in minimum essential medium with antioxidant-free B-27 (Invitrogen, Melbourne, Vic, Australia). In some experiments, treatment of neurons with STS or H_2O_2 was also performed in the presence of a broad-spectrum caspase inhibitor z-Val-Ala-Asp(OCH_3)-CH_2F (zVAD-fmk) (Bachem, Bubendorf,

Switzerland) at 100 μmol/l. Cells were pre-treated with zVAD-fmk in minimum essential medium with antioxidant-free B-27 30 min prior to treatment with STS or H_2O_2, with zVAD-fmk remaining in the medium during such subsequent treatments.

Cell viability

Cells from cultures were directly stained with 5 μg/ml of propidium iodide (PI) (Invitrogen-Molecular probes, Melbourne, Vic, Australia) in 1 × phosphate buffered saline, pH 7.4 (PBS). Following incubation for 5 min at 37°C, cells stained with PI were washed three times with 1 × PBS before being fixed with 3% paraformaldehyde in 1 × PBS at 22°C, before being mounted on glass slides [10, 29].

Nuclear morphology and TUNEL

Staining of nuclei with 4′,6-diamidino-2-phenylindole (DAPI; Invitrogen-Molecular Probes, Melbourne, Vic, Australia) was carried out as described [10] and morphology determined by confocal microscopy (see below). TUNEL staining was carried out using a TUNEL kit (Promega, Alexandria, NSW, Australia). Where DAPI was used in conjunction with TUNEL, DAPI was incubated with the samples following completion of TUNEL procedure for 5 min at 22°C; samples were then washed with 1 × PBS twice before mounting samples onto glass slides.

Immunocytochemistry

Immunocytochemistry was performed as described [29]. In the present work, following fixation and permeabilization, samples were then incubated with the following primary antibodies at optimal dilutions for 3 h at 22°C: rabbit polyclonal anti-active caspase-3 antibody at 1:500 (Neuromics, Edina MN); rabbit polyclonal anti-cleaved caspase-7 antibody at 1:100 (Cell Signaling, Danvers, MA); mouse monoclonal anti-cytochrome *c* (cyt *c*) antibody (clone 2410 6H2.B4) at 1:200 (BD Pharmingen, San Diego, CA); mouse monoclonal anti-AIF antibody (clone E-1) at 1:200 (Santa Cruz, CA); or rabbit polyclonal anti-Endo G antibody at 1:200 (Pro-Sci Inc, Poway, CA). Following incubation with the primary antibody, samples were processed as described [29].

Determination of mitochondrial polarization

Uptake of tetramethylrhodamine methyl ester (TMRM) (Invitrogen-Molecular Probes, Melbourne, Vic, Australia) into live neurons in culture was determined as described [10, 11]. In the present experiments cells were loaded with TMRM (150 nmol/l) after particular times of prior treatment with STS or H_2O_2. After washing cells with PBS, TMRM was maintained during subsequent incubation in minimum essential medium, without phenol red, prior to and during imaging. A depolarization control sample [10 μmol/l; Carboxy cyanide p-(trifluoromethoxy)phenylhydrazone (FCCP), Invitrogen-Molecular Probes, Melbourne, Vic, Australia] was also included, where relevant. Cells on coverslips were imaged directly by confocal microscopy.

Confocal microscopy

Samples were imaged by fluorescence laser scanning confocal microscopy using an Olympus FluoView500, IX81 inverted confocal microscope (Olympus, Melbourne, Vic, Australia), fitted with a UPlan Apo 60 ×/1.20w water immersion lens. Images were captured using Fluroview software (Olympus, Melbourne, Vic, Australia). In multiple fluorescence channel imaging, photomultiplier sensitivities, gain levels and offsets were adjusted to ensure that there was little or no bleed-through of fluorescence signal from one channel to the other. A Kalman filter was used to reduce background noise levels. The selected field was scanned five times using a "Frame Kalman" scan. All fields were scanned sequentially in order to reduce the incidence of 'bleed through' between each of the channels used. Three hundred cells were scored for each population scored, and three independent experiments were undertaken for each condition tested. Image Tool Software Ver 3.00 (developed by the Department of Dental Diagnostic Science at The University of Texas Health Science Center, San Antonio, Texas) was used to assist manual scoring of cellular morphologies.

Caspase-3 and caspase-7 fluorescence activity assays

Caspase-3 activity was measured directly by examining the binding of a FITC-DEVD-fmk substrate (Calbiochem, Kilsyth, Vic, Australia) to active caspase-3 in attached cells. Neurons were cultured in 96-well plates (0.1×10^6) and processed according to the manufacturer's instructions. Cellular fluorescence was measured in relative fluorescence units (RFU) (excitation 485 nm/emission 530 nm), using a Fluorostar Optima plate reader (BMG Labtech, Mornington, Vic, Australia).

A caspase-7 fluorogenic/immunoassay kit (Calbiochem, Kilsyth, Victoria, Australia) was used to measure active caspase-7 in neurons. As per manufacturer's instructions, cell lysates were first prepared in each well of the microtiter plate, and lysates were then applied to other 96-well plates coated with a polyclonal caspase-7 antibody,

thereby to capture caspase-7. The adhered material in the well was then exposed to a DEVD-AFC substrate in the supplied buffer. The fluorescence of the bound substrate was measured in RFU (excitation 405 nm/emission 510 nm). Recombinant caspase-7 provided with the kit was used as the positive control.

Western immunoblotting

Following treatment with H_2O_2 and STS, cells were harvested by gentle scraping and centrifugation (800 g, 5 min) and treated with RIPA extraction buffer [10 mM Tris-HCl pH 8.0, 150 mM NaCl, 1% NP-40, 1% sodium deoxycholate, 0.1% SDS; protease inhibitor cocktail (Sigma-Aldrich, Castle Hill, NSW, Australia) was also added] for 5 min at 4°C. The supernatant obtained by centrifugation (15,000*g*, 15 min) at 4°C was retained for WB analyses. The protein concentration of supernatants was determined using a BCA Protein Assay Kit (Pierce). The proteins were denatured in Laemmli sample buffer (Bio-Rad, Hercules, CA) at 95°C for 5 min, and separation was carried out on a 12% NuPAGE Bis-Tris pre-cast gel (Invitrogen, Melbourne, Vic, Australia) where the protein ladder (10 µl) and sample (20 µl, 15–20 µg total protein) were separated at 200 V for 30 min. Routine procedures were used for transfer, washing, blocking and probing of blots. Membranes were incubated overnight at 4°C with either primary rabbit polyclonal anti-Endo G antibody (1:1,000; Pro-Sci Inc, Poway, CA), rabbit polyclonal anti-caspase-3 and anti-caspase-7 antibodies (1:1,000; Cell Signaling, Danvers, MA) or mouse monoclonal anti-β-actin antibody (1:400, Neomarkers, Fremont, CA) in 3% blotting reagent. Secondary Alexa488-labeled antibody (1:1,000; Invitrogen-Molecular Probes, Melbourne, Vic, Australia) was incubated for 2 h at room temperature. Visualization of specific bands was performed using a Typhoon Trio^{TM} scanning system (GE Healthcare Life Sciences, Bundoora, Vic, Australia). Densitometry of the western immunoblot was performed using the Image-Quant^{TM} TL software suite (GE Healthcare Life Sciences, Bundoora, Vic, Australia).

Statistical analysis

Comparative data sets were analyzed statistically by using one- and two-way ANOVA, followed by Bonferroni's post hoc test (GraphPad Prism, San Diego, CA). One-way ANOVA was used for intra-group analysis, while two-way ANOVA was carried out to compare populations subjected to different treatments. The results are expressed as the mean ± SEM. The differences were considered significant at $P < 0.05$.

Results

General features of cell death induced by STS and H_2O_2

Cell death induced by STS or H_2O_2 was determined by scoring neurons for PI uptake, indicative of compromised PM integrity (Fig. 1a, upper rows). A steady increase in cell death over the course of 24 h consistent with the progression of apoptosis was observed after STS treatment (Fig. 1b). In contrast, H_2O_2 treatment induced a more rapid death; about 60% of cells took up PI after 4 h (Fig. 1b). After both treatments, in contrast to untreated neurons, the cells exhibited retracted neurites and condensed cell bodies (in proportion to PI uptake), but not the rapid cellular swelling (0.5–2 h) that is associated with necrosis.

Changes in nuclear morphology provide a basis for characterizing the mode of death. Apoptotic death in these neurons was measured by scoring neurons with condensed nuclei after DAPI staining, and DNA fragmentation was assessed using TUNEL. Neurons treated with STS exhibited condensed nuclei, which almost invariably showed a fragmented morphology typical of apoptosis (Fig. 1a, lower rows). The proportion of cells exhibiting these features increased with time, in parallel with PI uptake (Fig. 1b). On the other hand, neurons treated with H_2O_2 mostly exhibited condensed rounded nuclei with minimal fragmentation evident (Fig. 1a, lower rows). The incidence of such condensation over time was delayed relative to PI uptake at 4 h, where only 40% of nuclei were condensed, but this proportion doubled to about 80% after 12 h, comparable to PI uptake (Fig. 1b). When relatively high frequencies of condensed nuclei were observed, the proportion of nuclei that were both condensed and fragmented was found to be only about 1–2% (data not shown). These results raise the possibility that more than one type of cell death maybe occurring in response to H_2O_2 treatment.

Quantification of TUNEL-positive neurons confirmed the incidence of apoptotic death in response to STS treatment (Fig. 1a, lower rows). The incidence of DNA fragmentation in response to STS treatment increased at the same rate as those of nuclear condensation/fragmentation and PI uptake (Fig. 1b). Insult with H_2O_2 also induced DNA fragmentation monitored by TUNEL, but over the first 12 h this occurred at a slower rate than that seen for nuclear condensation ($P < 0.01$ ANOVA). However, these indices of nuclear modification reached similarly high levels (70–80%) after 24 h (Fig. 1b). The temporal dependence of PI uptake seen after exposure to H_2O_2 was significantly different to that observed as a consequence of treatment with STS (4 h and 12 h, $P < 0.001$ ANOVA). Taken

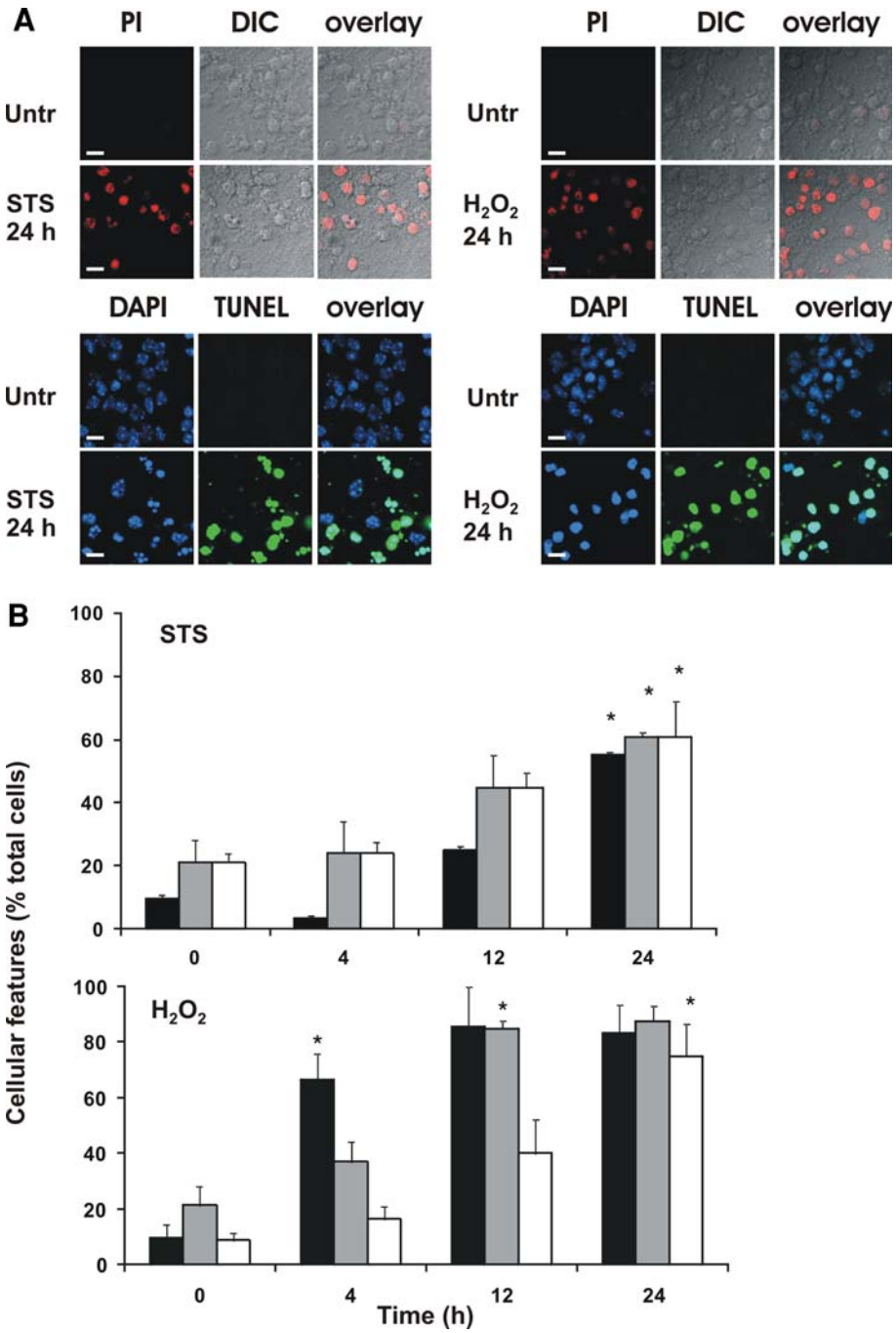

Fig. 1 Features of cell death induced by staurosporine (STS) and hydrogen peroxide (H_2O_2) in primary cortical neurons. Neurons were treated for various times at which were determined the uptake of PI, the morphology of nuclei after DAPI staining and DNA fragmentation by TUNEL. **a** Upper two rows show images of cells stained with PI, together with differential interference contrast (DIC) images of the same field. Images are shown for untreated (Untr) neurons and those treated with STS or H_2O_2 for 24 h. Lower two rows show images of nuclei stained with DAPI and, for the same fields, labeled with TUNEL. Treatments were as above. *Bars* represent 10 μm. **b** Quantitative analysis of temporal changes in treated populations. *Black bars*, PI uptake; *grey bars*, condensed nuclei; *white bars*, TUNEL labeling. Data for each population scored represent the mean percentage of cells scored for each feature ($n = 300$–500 for each population). Values are mean ± SEM of three independent experiments. *Asterisks* indicate the earliest time point for a given feature that displays significant difference ($P < 0.05$) comparing a treated population with the relevant untreated control at time zero h

together with the previous observation that loss of membrane integrity occurs faster than nuclear condensation at early times of H_2O_2 exposure, the data obtained for nuclear modification indicate that the cell death pathways invoked by H_2O_2 appear to be distinct from those corresponding to apoptosis. While some apoptosis is occurring in these dying neurons, the morphology of nuclei and the kinetics of DNA fragmentation monitored by TUNEL differ from those features seen with STS.

Mitochondrial membrane potential changes distinctly following STS or H_2O_2 treatment of neurons

Changes in mitochondrial membrane potential ($\Delta\Psi_m$) during treatment were studied using live cell imaging by monitoring the retention of the dye TMRM within mitochondria. TMRM fluorescence was visible within mitochondria in untreated control neurons and was efficiently dissipated with the uncoupler FCCP that collapses

$\Delta\Psi_m$ (Fig. 2a). Whereas STS-treated neurons showed strong fluorescence (in excess of that of untreated control cells, suggesting mitochondrial hyperpolarization), H_2O_2-treated cells showed almost complete depolarization of mitochondria (Fig. 2a, third row). Following correction of fluorescence for that of the FCCP-treated cells, TMRM fluorescence was quantified in the drug-treated populations over 4 h. Such quantification revealed that STS indeed invoked hyperpolarization of mitochondria (elevated $\Delta\Psi_m$) at 1 h (Fig. 2b), as often occurs during apoptosis induced by this drug [30]. After 4 h, fluorescence declined to that of untreated controls, possibly reflecting cyt *c* redistribution from mitochondria [31]. By contrast, a severe loss of $\Delta\Psi_m$ occurred within the first hour of treatment with H_2O_2 ($P < 0.001$ ANOVA), and by 4 h, almost total depolarization of mitochondria had occurred (Fig. 2b). While depolarization, as such, is not a defining characteristic of apoptosis [30], the data show the mitochondrial response to STS and H_2O_2 to be quite different.

Caspase-3 and caspase-7 are minimally activated in response to oxidative stress

Downstream effector caspase-3 and caspase-7 were studied for activation to shed further light on the mode of cell death under oxidative insult. Single cell analysis was applied to determine the percentage of cortical neurons that reveal activated (cleaved) caspase-3 during cell death. Immunocytochemistry was used to identify neurons with cleaved caspase-3 (Fig. 3a). A proportion of STS-treated cells became labeled with antibody specific for activated caspase-3 (Fig. 3a). Quantification of such labeled neurons shows 30% activation by 24 h (Fig. 3b). However, scoring of neurons treated with H_2O_2 revealed negligible cleavage of caspase-3 compared to the untreated population (Fig. 3a and b).

Caspase-3 activity measurements using FITC-DEVD-fmk substrate were applied to confirm the activation of this enzyme in STS-treated neurons but not in those treated with H_2O_2 (Fig. 4a). Significantly, these assays also showed that progress towards caspase-3 activation induced by STS is strongly inhibited by the pan-caspase inhibitor z-VAD-fmk (Fig. 4a), confirming that these cultured cortical neurons are indeed capable of activating caspase-3. The dependence of these neurons on caspase-3 for apoptosis is not clear, because the single cell analysis (Fig. 3b) revealed STS treatment to induce caspase-3 activation in only 30% of cells after 24 h, despite 80% of neurons undergoing both nuclear DNA changes and cell death (Fig. 1b).

Studies of the apoptotic pathways in cells of C57/Black 6 J mice lacking caspase-3 revealed caspase-7 to be an

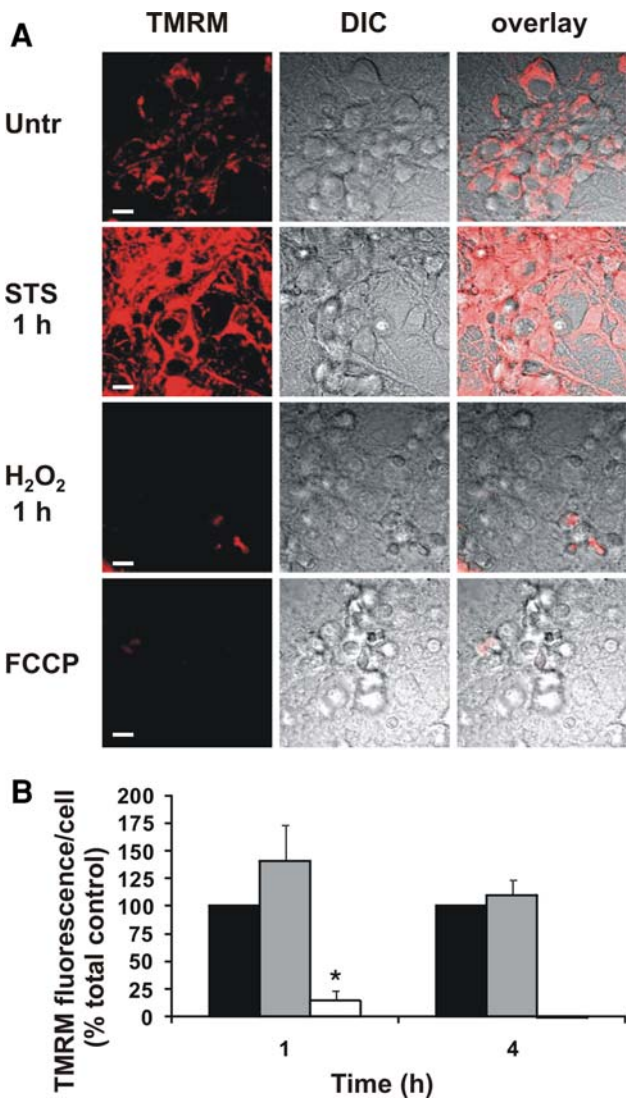

Fig. 2 Polarization of mitochondria during treatment of cortical neurons with staurosporine (STS) and hydrogen peroxide (H_2O_2). Neurons were treated for various times at which cells were loaded with TMRM and the live cells imaged by confocal microscopy. **a** Images of neurons loaded with TMRM, in untreated (Untr), or after treatment with STS or H_2O_2 for 1 h. FCCP was applied to neurons loaded with TMRM as a control for complete depolarization. DIC images are also included to visualize depolarized cells. Bars represent 10 μm. **b** Quantitative analysis of intracellular TMRM fluorescence intensity in STS-treated and H_2O_2-treated neurons. This was carried out by aggregating total pixel intensity across a given field divided by the number of cells in that field (determined by the DIC image). The raw values for treated neurons were normalized to fluorescence intensity/cell of untreated neurons (expressed as a percentage). For this purpose 400–600 cells were scored in each treatment condition. All values were previously corrected for residual TMRM fluorescence after FCCP treatment. *Black bars*, untreated; *grey bars*, STS; *white bars*, H_2O_2. Values are mean ± SEM of three independent experiments. *Asterisk* indicates the earliest time point for a given feature that displays a significant difference ($P < 0.0001$) comparing a treated population with the relevant untreated control

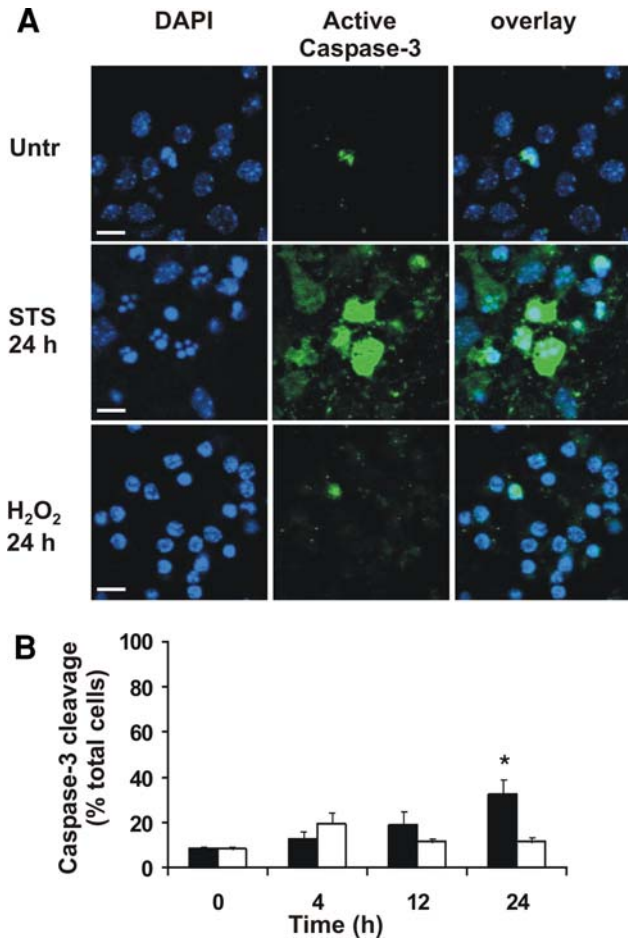

Fig. 3 Caspase-3 activation during staurosporine (STS) and hydrogen peroxide (H_2O_2) treatment. **a** Antibody specific for activated caspase-3 was used to immunolabel neurons. DAPI was used as a counterstain for nuclei to determine the total number of cells per field. Other indications as for Fig. 1a. **b** Quantitative analysis of treated populations. *Black bars*, STS; *White bars*, H_2O_2. Data for each population scored represent the mean percentage of cells scored for caspase-3 activation ($n = 300$–500 for each population). Values are mean ± SEM of three independent experiments. *Asterisk* indicates the earliest time point for caspase-3 activation that displays significant difference ($P < 0.001$) comparing a treated population with the relevant untreated control at time zero h

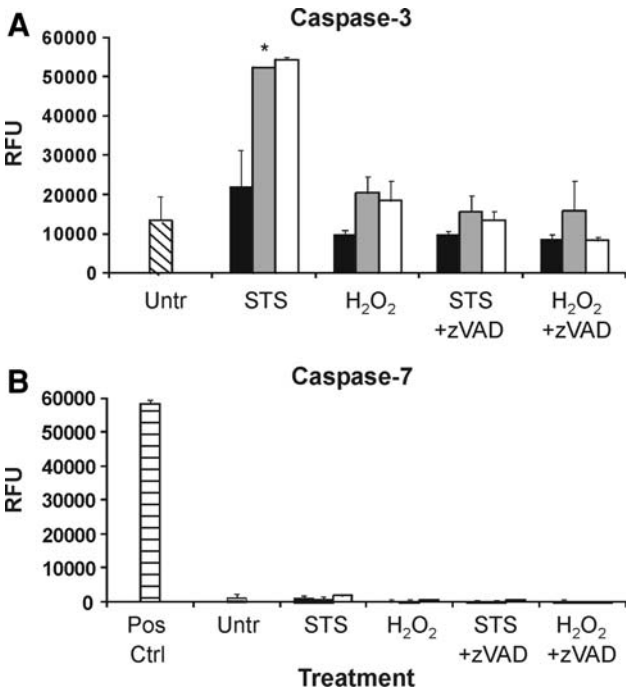

Fig. 4 Caspase-3 and caspase-7 activity measured by fluorescence of bound substrate analogs. Neurons were treated in microtiter plates, for various times at which the attached cells were subjected to caspase activity tests. **a** Caspase-3 activity measured during treatments with STS or H_2O_2; in some populations zVAD-fmk (indicated by +zVAD) was additionally included during the treatment. Diagonally striped bar, untreated (Untr); *black bars*, 4 h; *grey bars*, 12 h; *white bars*, 24 h. Fluorescence intensities are indicated as relative fluorescence units (RFU). *Asterisk* indicates the earliest time point for a given feature that displays significant difference ($P < 0.001$) comparing a treated population with the relevant untreated control. **b** Caspase-7 activity measured during treatment using a capture procedure for this enzyme. All indications as for Fig. 3a; additionally, horizontally *striped bar* represents positive control in this assay (Pos Ctrl). Data for each treatment condition and time represent mean ± SEM of three independent experiments, each carried out in triplicate wells on a single microtiter plate

alternative downstream caspase activated during cell death [32]. Therefore, a caspase-7 fluorogenic/immunoassay was used here to determine caspase-7 activity in primary cultured cortical neurons treated with STS or H_2O_2. Neither insult was observed to induce activated caspase-7 up to 24 h treatment (Fig. 4b), although a control sample containing activated caspase-7 showed a strong signal. These observations suggest that these cortical neurons show minimal activation of caspase-7 after either treatment with STS or H_2O_2. Since neither caspase-3 or caspase-7 is activated during the cell death induced by H_2O_2, it can be concluded that a death pathway distinct from apoptotic PCD-type I occurs after severe oxidative stress.

Redistribution of IMS proteins from mitochondria occurs during H_2O_2-induced cell death

To characterize the neuronal death process in more detail, involvement in cell death of apoptogenic mitochondrial proteins was assessed for both STS and H_2O_2. Cyt c, Endo G and AIF in treated neurons were studied using immunocytochemistry and confocal microscopy to establish the timing of redistribution from mitochondria of these pro-death proteins that normally reside in the IMS. As in previous work with immunocytochemical analysis of cyt *c* redistribution [10, 29], Endo G was scored as having been redistributed when the fluorescent signal changed from punctuate (i.e., localized to mitochondria) with a clearly evident nuclear void in the cellular fluorescence (Fig. 5a, upper row) to a dispersed distribution of fluorescence within the cell also covering the nucleus (marked by DAPI;

Fig. 5a, lower row). Due to the rounded morphology of treated neurons, it was not possible to discern whether Endo G was entirely localized to the nucleus or retained some cytosolic distribution. Comparable images for AIF redistribution from mitochondria are shown in Supplementary Fig. 1.

Cyt c, Endo G and AIF were all found to be released from mitochondria progressively over 24 h in response to STS at a similar rate. Thus, at 24 h, redistribution occurred in more than 60% of neurons for cyt *c* and AIF (tested separately) ($P < 0.05$ ANOVA). At this time a slightly smaller proportion of cells (about 50%) has undergone redistribution of Endo G ($P < 0.05$ ANOVA) (Fig. 5b). The timing of release of these pro-death proteins from mitochondria in response to STS treatment is characteristic of apoptotic cell death, in relation to the timing of changes in nuclear morphology and the loss of membrane integrity (Fig. 5b).

By contrast, in response to H_2O_2 the neurons showed significant early redistribution for all three proteins ($P < 0.05$ ANOVA). Thus, at 4 h, more than 70% of H_2O_2-treated cells had undergone redistribution of cyt *c* (Fig. 5b). At this time point, each of Endo G and AIF (scored separately) showed redistribution in about 50% of treated cells. This early redistribution of these pro-death proteins occurred in parallel with the more rapid loss of PM integrity (PI uptake) seen in response to H_2O_2 as opposed to STS (Fig. 1b). The timing of Smac/DIABLO redistribution was also studied; this protein was shown to be released from mitochondria more or less concordantly with cyt *c* in response to both STS and H_2O_2 (data not shown). Exposure of cells to the inhibitor z-VAD-fmk during treatment with STS and H_2O_2 had no discernable effect on the redistribution kinetics of cyt *c*, AIF or Endo G (data not shown). This outcome may be explained by a lack of caspase activation, as demonstrated above in the previous section.

Suppression of cellular levels of Endo G delays nuclear modifications during H_2O_2 treatment

The lack of caspase activation in H_2O_2-treated neurons raises the question of the role of Endo G in the nuclear modifications seen during severe oxidative stress. In order to study the dependence on Endo G of nuclear modifications in terms of morphology and DNA fragmentation, siRNA was used to silence expression of Endo G. Knockdown of Endo G greater than 60% was routinely achieved with siRNA specific for Endo G mRNA (siEndoG) under conditions where non-specific RNA (nRNA)

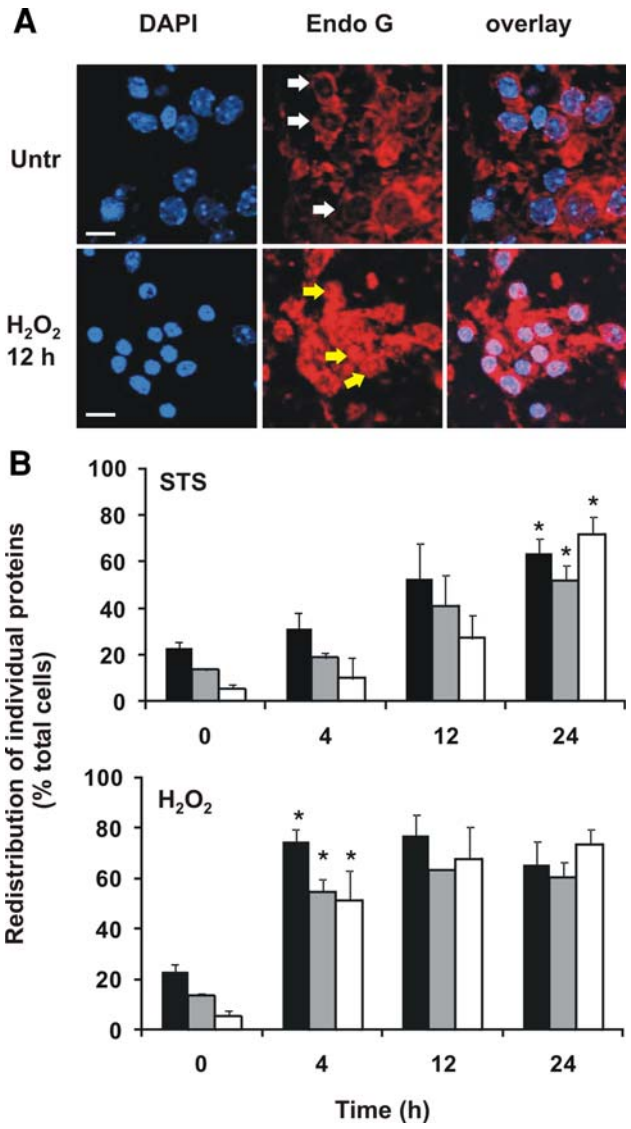

Fig. 5 Redistribution of IMS from mitochondria in cortical neurons during staurosporine (STS) and hydrogen peroxide (H_2O_2) treatment. Localization of individual proteins was determined by immunocytochemistry and confocal microscopy. **a** Endonuclease G (Endo G) redistribution from mitochondria. Cells were immunostained for Endo G and counterstained with DAPI to visualize nuclei. *Top row* shows untreated neurons with Endo G localized to mitochondria, with nuclear void visible in immunostain (*white arrows*). *Lower row* shows neurons after H_2O_2 treatment for 12 h with Endo G redistributed across the nucleus (*yellow arrows*). **b** Quantitative analysis of temporal changes in protein redistribution. Neurons were scored for redistribution of cytochrome *c* (cyt *c*; *black bars*), Endo G (*grey bars*) and apoptosis-inducing factor (AIF; *white bars*). Data for each population scored represent the mean percentage of cells scored for each IMS protein ($n = 300$–500 for each population). Values are mean ± SEM of three independent experiments. *Asterisks* indicate the earliest time point for the redistribution of a given IMS protein that displays significant difference ($P < 0.05$) comparing a treated population with the relevant untreated control at time 0 h

induced little or no change in cellular Endo G levels (Fig. 6a). Individual replicate experiments showed knockdown in the range 60–80% (data not shown). Changes in nuclear morphology and DNA fragmentation were monitored in neuronal populations transfected with control nRNA and siEndoG. For cells treated with STS, siEndoG showed some impairment in the progression of nuclear morphology changes at early times, but by 24 h there was no overall inhibition (Fig. 6b and c). The siEndoG had no effect on the progression of DNA fragmentation monitored by TUNEL (Supplementary Fig. 2A and B). This weak dependence in STS-treated cells on Endo G for nuclear modification is consistent with the activation of caspase-3, as these nuclear changes presumably mostly result from caspase-activated DNases. However, in the case of H_2O_2-treated cells, siEndoG substantially reduced the proportion of cells displaying condensed nuclei (Fig. 6b). Quantification showed suppression of nuclear morphology changes at all time points tested during H_2O_2 treatment (Fig. 6c) ($P < 0.001$, ANOVA). DNA fragmentation (TUNEL) was also significantly reduced after H_2O_2 treatment of neurons transfected with siEndoG relative to nRNA-transfected controls (Supplementary Fig. 2A and B) (24 h, $P < 0.001$, ANOVA). These findings demonstrate the dependence of neurons on Endo G in inducing nuclear modifications after H_2O_2 insult, but not after exposure to STS.

AIF has been well documented as another caspase-independent modulator of cell death in primary neurons [13, 20, 33]. To begin addressing its role in H_2O_2-induced nuclear modifications during cell death, AIF knockdown using siRNA (siAIF) was achieved in these cortical neurons (Supplementary Fig. 3A). However, it was found that when such siAIF-transfected neurons were placed in antioxidant-free medium, as routinely used in these studies, the majority of cells (over 80%) died prior to treatment with STS or H_2O_2 (Supplementary Fig. 3) ($P < 0.0001$, ANOVA). This outcome prevented any further investigation here into the role of AIF in cell death. Interestingly, these findings suggest that these cortical neurons may be dependent on the oxidoreductase activity of AIF as a key part of their antioxidant defense mechanism, as previously shown in other studies [23, 24].

Silencing of Endo G suppresses cell death in cortical neurons during H_2O_2-treatment

The role of Endo G in inducing cell death, as such, in cortical neurons was also studied to determine if this protein is a key component of PCD-type III under H_2O_2 insult. Therefore, siEndoG or nRNA were introduced into neurons

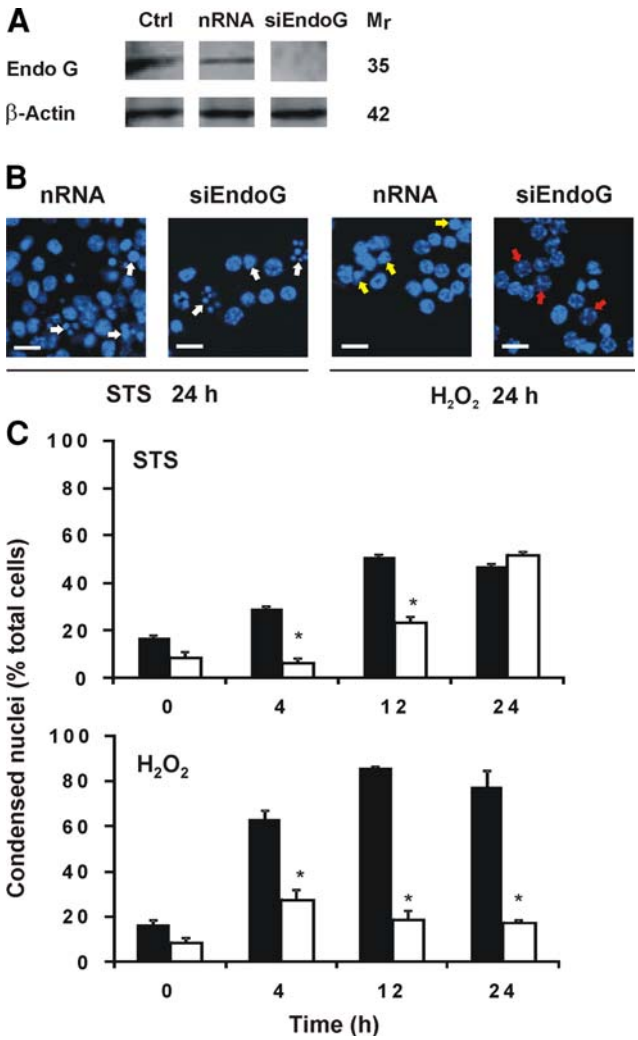

Fig. 6 Changes in nuclear morphology in staurosporine (STS)-treated and hydrogen peroxide (H_2O_2)-treated cortical neurons transfected with siRNA to suppress Endo G (siEndoG) and non-silencing siRNA (nRNA). **a** Western immunoblots of Endo G in cell lysates with β-actin as loading control. Lanes indicate untransfected control (Ctrl), and cells transfected with nRNA or siEndoG. Sizes of proteins visualized (kDa) are indicated at right. Representative gel shown here indicates greater than 80% suppression of Endo G by siEndoG. **b** Nuclear morphology revealed by DAPI staining of neurons after STS or H_2O_2 treatment for 24 h. Neurons transfected with nRNA displayed condensed nuclei after treatment with either STS (indicating condensed and fragmented nuclei, *white arrows*) or H_2O_2 (indicating condensed nuclei, *yellow arrows*). Neurons transfected with siEndoG exhibited condensed and fragmented nuclei 24 h after STS treatment (*white arrows*), but not after H_2O_2 treatment (non-condensed nuclei, *red arrows*). Bars represent 10 µm. **c** Quantitative analysis of nuclear morphology changes in transfected cells after treatment with STS or H_2O_2. *Black bars*, nRNA; *white bars*, siEndoG. Results shown here report triplicate analyses within a single experiment. Due to the variation in Endo G suppression achieved between experiments (see text), similar data obtained from three replicate experiments were not combined for quantification here. *Asterisks* indicate time points where there was significant difference between nRNA and siEndoG populations ($P < 0.001$)

before treatment with STS and H_2O_2, monitoring loss of PM integrity by PI uptake. The siEndoG showed no suppression of cell death after 24 h of STS treatment (Fig. 7a), although at earlier time points there was some delay in progression of STS-treated cells to death (Fig. 7b) ($P < 0.001$, ANOVA). In contrast, siEndoG almost completely suppressed cell death at all time points tested up to 24 h treatment with H_2O_2 (Fig. 7a and b) ($P < 0.001$, ANOVA). These results show that H_2O_2 induced a discrete form of PCD in these neurons, with Endo G shown to be a key modulator of this cell death cascade. Endo G may also have a minor role modulating apoptosis in STS-treated neurons.

Discussion

Features of neuronal cell death pathways under oxidative stress

Oxidative stress is a key trigger of cell death following ischemic reperfusion during stroke [34] and has also been implicated in other neurodegenerative diseases. Mitochondria are a suitable target for cell death investigations, not only because of their recognized role in cell death signaling, but also because they are a significant source of ROS generation during episodes of neuronal dysfunction [35]. In this study the cell death pathway triggered by H_2O_2 was

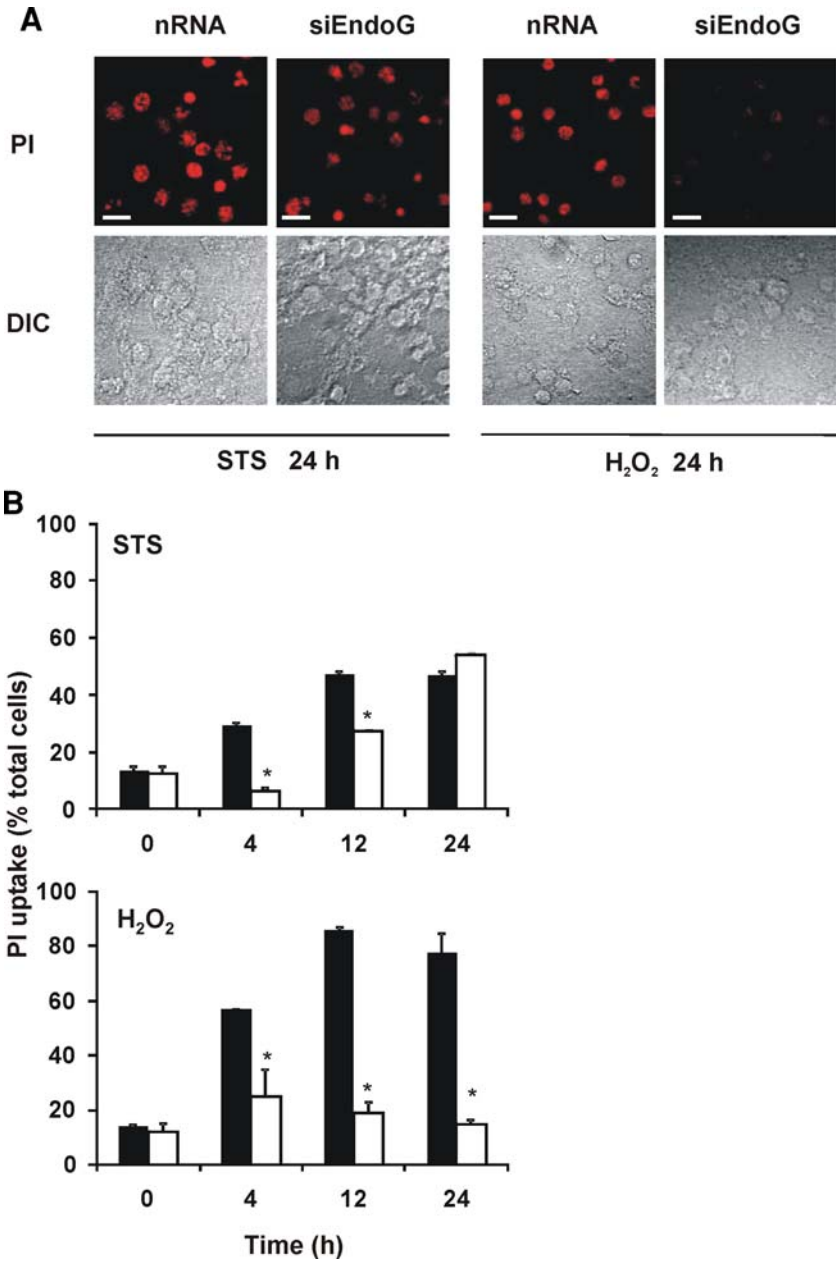

Fig. 7 Cell death in staurosporine (STS)-treated and hydrogen peroxide (H_2O_2)-treated cortical neurons transfected with siRNA to suppress Endo G (siEndoG) and non-silencing siRNA (nRNA). **a** PI uptake in images of transfected cortical neurons after treatment with either STS or H_2O_2 for 24 h. DIC images are provided to visualize the total number of cells in each field. *Bars* represent 10 μm. **b** Quantitative analysis of PI uptake in transfected cells after treatment with STS or H_2O_2. All other indications as for Fig. 6c

characterized in order to determine whether cell death under these conditions is a programmed event or has the features characteristic of unregulated necrosis. Concurrent observations of injury characteristics were made with STS (an apoptotic inducer). We thereby demonstrated that in cortical neurons from C57 Black/6 J embryonic mice, STS induced a process with features of apoptosis (PCD-type I), namely delayed PM permeabilization, clear evidence of nuclear condensation and morphological fragmentation, as well as differential redistribution of apoptogenic IMS proteins (Fig. 8). However, activation of caspase-3 activity was relatively low. On the other hand, H_2O_2 induced a PCD-type III scenario involving disruption of $\Delta\Psi_m$ and rapid loss of PM integrity, widespread nuclear condensation but without overt fragmentation, and redistribution of apoptogenic IMS proteins featuring early cyt *c*, Endo G and AIF release. Moreover, mitochondrial release of Endo G was shown to play a deterministic role, but no involvement of either caspase-3 or caspase-7 could be demonstrated (Fig. 8). The results are thus consistent with previous findings that H_2O_2 could trigger cell death in the absence of downstream caspase activity in some neuronal systems, depending on the insult intensity [36–38].

The present findings clearly emphasize the differential recruitment of mitochondria and their intrinsic pathway during cell death in neurons under STS and H_2O_2 treatments, and more precisely define the nature of the different PCD pathways under each insult. The lack of downstream caspase activation in response to H_2O_2, despite the release of cyt *c*, heightened the significance of AIF and Endo G redistribution under this insult. We showed explicitly that siRNA silencing of Endo G expression inhibited H_2O_2-induced cell death, revealing Endo G as a necessary executioner, and programmed necrosis (or PCD-type III) as the death pathway invoked, rather than unregulated necrosis under these conditions. By contrast, silencing of Endo G expression only delayed STS-induced cell death, confirming activation PCD-type I and suggesting that Endo G plays an ancillary role in apoptotic outcomes under these conditions.

The mechanisms that regulate PCD-type III for the most part are poorly defined. This scenario is largely due to its sharing similar features with unregulated necrosis. In the latter, more traumatic, cell response leading to death, it would be unlikely that silencing a known death-inducing protein (such as Endo G) would prevent or significantly

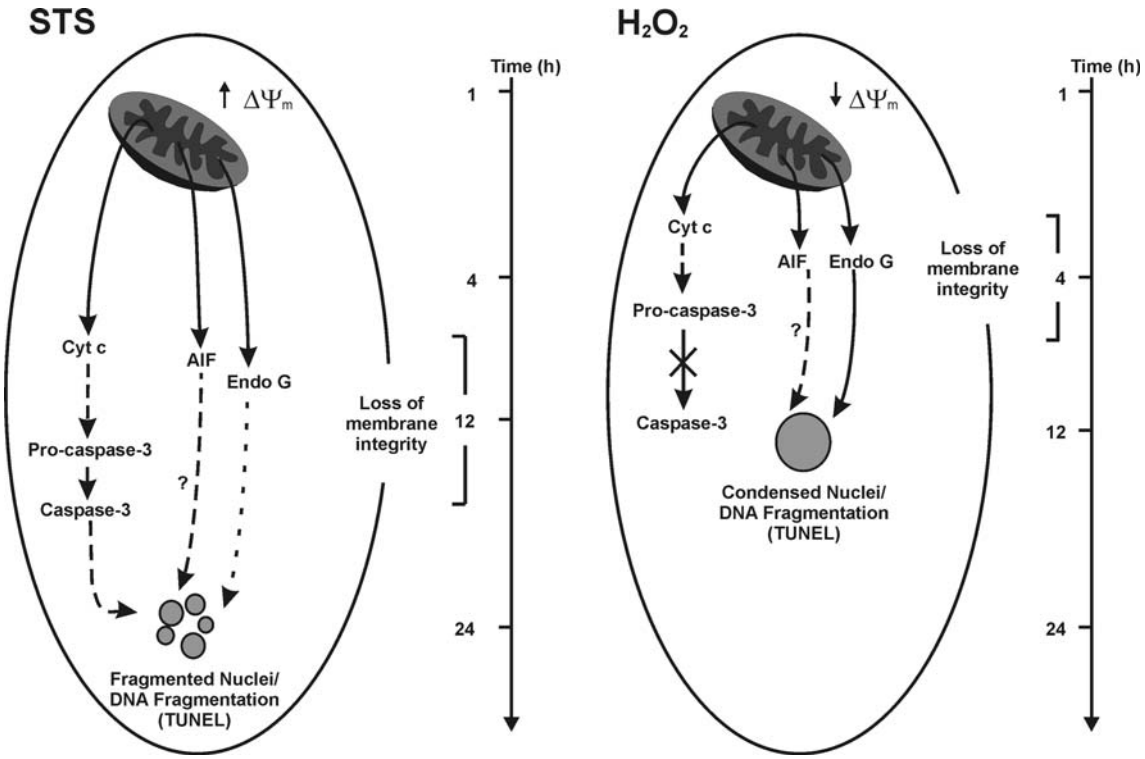

Fig. 8 Schematic representation of cellular events in the two types of PCD and their timelines in primary cortical neurons treated with STS (PCD-type I) and H_2O_2 (PCD-type III). *Solid arrows* represent events that have been empirically defined in the present work. *X* indicates one such step, namely caspase-3 activation not to be effected under H_2O_2 treatment. *Dashed arrows* represent events that are known to occur in these types of treated cells, as demonstrated by other studies (references cited in text). *Dotted arrows* indicate events that are inferred to have an ancillary role in cell death (see text). Question mark indicates a possible role for AIF in these treated cells, but this could not be experimentally validated here

slow the death process. In a recent reclassification of cell death pathways [39], alternative names were considered for the various death processes, comparable to the PCD nomenclature used here. In these terms, one subtype of programmed necrosis is termed "necroptosis," which broadly covers the definition of PCD-type III. Necroptosis is distinct from other forms of programmed necrosis in that it depends on the activity of receptor interacting protein-1 (RIP-1) [40]. Necroptosis has been demonstrated to be involved in delayed cell death after ischemic brain injury in mice, which can be blocked by the necroptosis inhibitor, necrostatin-1 (Nec-1) [41]. Nec-1 has been shown to inhibit RIP-1 [42], as well as being capable of reducing ROS levels in neuronal cells, acting upstream of the ROS production, rather than scavenging ROS directly [41, 43]. Indeed the PCD-type III studied here may be necroptosis, and further investigation is warranted to investigate RIP-1 involvement. Moreover, based on our findings it would be worth determining whether Endo G is involved in all forms of programmed necrosis or only select subtypes. For example, it was recently shown that silencing of BNIP3 in rat primary cortical neurons during hypoxia prevented the redistribution of Endo G [44].

Deficits of caspase activation in C57/Black 6 J cortical neurons

STS treatment induced a classical apoptotic response that included the activation of caspase-3, but not caspase-7. The embryonic cortical neurons harvested from C57/Black 6 J mice appeared to have a predisposition towards caspase-independent cell death. The level of caspase-3 activation was lower than that previously reported during apoptosis in embryonic cortical neurons harvested from Swiss mice [10, 45], suggesting possible strain differences. A dependence on caspase-7 in the absence of active caspase-3, as has been reported in neurons of caspase-3 null mice [32], was also not evident here. Caspase-3 and caspase-7 null mice on a C57/Black 6 J background are viable, suggesting that these caspases are redundant during early embryonic development [46], which possibly explains the relatively weak manifestation of caspase activity seen in the embryonic neurons studied here.

The apparent deficit in caspase-3 activation seen here during H_2O_2 treatment might be the result of oxidation of the thiol group within the active cysteine of this enzyme, which has been demonstrated before with ROS in other non-neuronal systems [47, 48]. Other studies have suggested that H_2O_2 does not inhibit procaspase-3 activation directly, but rather through the inactivation of procaspase-9 further upstream in the cell death pathway. H_2O_2 has been reported to induce iron-mediated inhibition of procaspase-9 [49] or possibly depletion of ATP that is needed for proteolytic activation of caspase-9 [50]. We have found that caspase-9 is active in neurons after STS, but not H_2O_2 treatment (data not shown), suggesting that caspase-3 inhibition may be the result of caspase-9 deficiency upstream in the cell death cascade. These observations would also explain the lack of caspase activity despite the release of cyt *c* from mitochondria after H_2O_2 treatment. The lack of caspase recruitment in these neurons after H_2O_2 treatment has underscored the need for these cells to have other caspase-independent pathways that can enact PCD.

Individual roles for Endo G and AIF in caspase-independent cell death of neurons

Endo G has been reported by some to reside within the mitochondrial matrix, tethered to the inner membrane, where it was thought to be involved in either mitochondrial DNA synthesis or eliminating mitochondrial DNA damage [51–53]. Others have shown evidence that Endo G resides within the IMS, from which it can be redistributed with other IMS proteins during cell death [21, 22, 54]. These discrepancies in defining the localization of Endo G may be specific to the cell type or even species. We observed Endo G redistribution from mitochondria, which was somewhat delayed relative to that of cyt *c* after both STS and H_2O_2 treatments.

During PCD, Endo G is thought to relocate to the nucleus where it is involved in caspase-independent cleavage of chromatin and DNA. There has been some uncertainty as to whether Endo G is in fact a critical part of PCD. While Endo G has been claimed to have no discernable involvement in apoptosis in cells from Endo G-null mice [51, 55], others have shown that it plays a role in caspase-independent apoptosis [21, 22, 56]. We showed here that Endo G does have a critical role in caspase-independent cell death induced by H_2O_2, but not in STS-treated neurons (see above). Here, Endo G was shown to induce downstream nuclear changes and ultimately cell death in the absence of caspase activity in cortical neurons under H_2O_2 insult. The redistribution of Endo G has been reported in several neuronal systems [57–59]. However, while Endo G redistribution has been shown to occur in each of these settings, none of these studies was able to confirm that Endo G was directly involved in cell death.

AIF has been the central focus of much research into caspase-independent neuronal cell death [11, 20, 23, 33] and has, in some respect, provided some focus for research on Endo G [60]. AIF is known to be responsible for causing DNA fragmentation independent of caspase activity during PCD [61]. One of the issues raised by the present work was the ability of siEndoG to inhibit cell death, while AIF was still putatively available as an executioner. The explanation

for this apparently critical role for Endo G may lie in the second function of AIF as an antioxidant, for which Endo G has no such demonstrated function. Thus, under oxidative stress, the oxidoreductase function of AIF is able to clear H_2O_2 [23]. It is plausible that AIF may have a primary function as an antioxidant, neutralizing H_2O_2 under conditions applied in the present work, which thereby obstructs it from performing its function a death executioner. This scenario may have facilitated a more dominant role for the alternative cell death signaling molecule Endo G. Our experience that ablation of AIF levels renders cells highly susceptible to oxidative stress induced death supports this view.

Differential response of mitochondria in neurons during PCD-type I and PCD-type III

We have shown that mitochondria have a central role in regulating PCD-type III (e.g., H_2O_2-treated neurons). Although mitochondria seem to play a similar role in PCD-type I (e.g., STS-treated neurons), they display contrasting kinetics in redistribution of apoptogenic proteins. It is likely that under H_2O_2 treatment the $\Delta\Psi_m$ loss seen was a result of the mitochondrial permeability transition (MPT) having been effected, which may have accelerated the redistribution of IMS proteins, particularly Endo G and AIF. Conversely, the redistribution of IMS proteins proceeded independently of any $\Delta\Psi_m$ loss during STS treatment, precluding the obligatory involvement of the MPT, in accordance with previous studies in many different systems [reviewed in 30, 62].

Perspectives on necrotic-type cell death in neurons

Following the onset of stroke, neuronal cell death has been thought to result from a combination of apoptosis and necrosis. While considerable attention has been paid to finding means by which apoptosis can be inhibited following stroke, necrosis has largely been overlooked due to it having been designated as an unregulated type of death. However, it is now apparent that some forms of necrosis in neurons could be regulated, in the sense that such death pathways are a systematic cellular response subject to molecular regulation. With oxidative stress and necrosis being implicated in other neurological disorders as well as stroke, it is possible that PCD-type III could be operative in many neuronal settings. Programmed necrosis has a number of potential advantages over passive (or "accidental") necrosis for the cell under threat of elimination, being more energy efficient, up-regulating anti-oxidant responses and inducing less inflammation [16, 63]. In the context of a tissue injury at the organismal level, these issues are currently most relevant to hypoxic-ischemic injury in the perinatal brain [16, 64]. Moreover, it is relevant that PCD is a dynamic process and that, dependent upon context, different PCD pathways (across the apoptosis-necrosis continuum) can operate in parallel or sequentially with multiple switch-points between them [65].

This prospect gives rise to the need for further research to be undertaken to determine if more precise and regulated mechanisms play roles in cell death previously identified as necrosis. Moreover, our study suggests that during episodes of oxidative stress, such as those associated with ischemic reperfusion injury, ensuing necrosis-like events in stroke may well be subjected to therapeutic interventions.

Acknowledgments We thank Ms Irene Hatzinisiriou for assistance with confocal microscopy and gel scanning, and Dr. Danielle Smith for technical advice. This work was supported by the National Health and Medical Research Council (Australia).

References

1. Jenner P (2007) Oxidative stress and Parkinson's disease. Handb Clin Neurol 83:507–520
2. Pratico D (2008) Evidence of oxidative stress in Alzheimer's disease brain and antioxidant therapy. Ann N Y Acad Sci 1147:70–78
3. Crack PJ, Taylor JM (2005) Reactive oxygen species and the modulation of stroke. Free Radic Biol Med 38:1433–1444
4. Saito A, Hayashi T, Okuno S, Ferrand-Drake M, Chan PH (2003) Overexpression of copper/zinc superoxide dismutase in transgenic mice protects against neuronal cell death after transient focal ischemia by blocking activation of the Bad cell death signaling pathway. J Neurosci 23:1710–1718
5. Vlessis AA, Widener LL, Bartos D (1990) Effect of peroxide, sodium, and calcium on brain mitochondrial respiration in vitro: potential role in cerebral ischemia and reperfusion. J Neurochem 54:1412–1418
6. Nelson CW, Wei EP, Povlishock JT, Kontos HA, Moskowitz MA (1992) Oxygen radicals in cerebral ischemia. Am J Physiol 263:H1356–H1362
7. Piantadosi CA, Zhang J (1996) Mitochondrial generation of reactive oxygen species after brain ischemia in the rat. Stroke 27:327–331 discussion 332
8. Fiskum G, Murphy AN, Beal MF (1999) Mitochondria in neurodegeneration: acute ischemia and chronic neurodegenerative diseases. J Cereb Blood Flow Metab 19:351–369
9. Dirnagl U, Iadecola C, Moskowitz M (1999) Pathobiology of ischaemic stroke: an integrated view. Trends Neurosci 22:391–397
10. Beart PM, Lim ML, Chen B, Diwakarla S, Mercer LD, Cheung NS, Nagley P (2007) Hierarchical recruitment by AMPA but not staurosporine of pro-apoptotic mitochondrial signaling in cultured cortical neurons: evidence for caspase-dependent/independent cross-talk. J Neurochem 103:2408–2427
11. Diwakarla S, Nagley P, Hughes ML, Chen B, Beart PM (2009) Differential insult-dependent recruitment of the intrinsic mitochondrial pathway during neuronal programmed cell death. Cell Mol Life Sci 66:156–172
12. Ward MW, Rego AC, Frenguelli BG, Nicholls DG (2000) Mitochondrial membrane potential and glutmate excitotoxicity in cultured cerebellar granule cells. J Neurosci 20:7208–7219

13. Wang H, Yu SW, Koh DW, Lew J, Coombs C, Bowers W, Federoff HJ, Poirier GG, Dawson TM, Dawson VL (2004) Apoptosis-inducing factor substitutes for caspase executioners in NMDA-triggered excitotoxic neuronal death. J Neurosci 24:10963–10973
14. Blomgren K, Leist M, Groc L (2007) Pathological apoptosis in the developing brain. Apoptosis 12:993–1010
15. Cheung NS, Pascoe CJ, Giardina SF, John CA, Beart PM (1998) Micromolar L-glutamate induces extensive apoptosis in an apoptotic-necrotic continuum of insult-dependent, excitotoxic injury in cultured cortical neurones. Neuropharmacology 37:1419–1429
16. Gill MB, Perez-Polo JR (2008) Hypoxia ischemia-mediated cell death in neonatal rat brain. Neurochem Res 33:2379–2389
17. Nicotera P, Melino G (2004) Regulation of the apoptosis-necrosis switch. Oncogene 23:2757–2765
18. Clarke PG (1990) Developmental cell death: morphological diversity and multiple mechanisms. Anat Embryol (Berl) 181:195–213
19. Henriquez M, Armisen R, Stutzin A, Quest AF (2008) Cell death by necrosis, a regulated way to go. Curr Mol Med 8:187–206
20. Cregan SP, Fortin A, MacLaurin JG, Callaghan SM, Cecconi F, Yu SW, Dawson TM, Dawson VL, Park DS, Kroemer G, Slack RS (2002) Apoptosis-inducing factor is involved in the regulation of caspase-independent neuronal cell death. J Cell Biol 158:507–517
21. Li LY, Luo X, Wang X (2001) Endonuclease G is an apoptotic DNase when released from mitochondria. Nature 412:95–99
22. van Loo G, Schotte P, van Gurp M, Demol H, Hoorelbeke B, Gevaert K, Rodriguez I, Ruiz-Carrillo A, Vandekerckhove J, Declercq W, Beyaert R, Vandenabeele P (2001) Endonuclease G: a mitochondrial protein released in apoptosis and involved in caspase-independent DNA degradation. Cell Death Differ 8:1136–1142
23. Klein JA, Longo-Guess CM, Rossmann MP, Seburn KL, Hurd RE, Frankel WN, Bronson RT, Ackerman SL (2002) The harlequin mouse mutation downregulates apoptosis-inducing factor. Nature 419:367–374
24. Zhu C, Wang X, Huang Z, Qiu L, Xu F, Vahsen N, Nilsson M, Eriksson PS, Hagberg H, Culmsee C, Plesnila N, Kroemer G, Blomgren K (2007) Apoptosis-inducing factor is a major contributor to neuronal loss induced by neonatal cerebral hypoxia-ischemia. Cell Death Differ 14:775–784
25. Crack PJ, Cimdins K, Ali U, Hertzog PJ, Iannello RC (2006) Lack of glutathione peroxidase-1 exacerbates Abeta-mediated neurotoxicity in cortical neurons. J Neural Transm 113:645–657
26. Farlie PG, Dringen R, Rees SM, Kannourakis G, Bernard O (1995) bcl-2 transgene expression can protect neurons against developmental and induced cell death. Proc Natl Acad Sci USA 92:4397–4401
27. Koh JY, Wie MB, Gwag BJ, Sensi SL, Canzoniero LM, Demaro J, Csernansky C, Choi DW (1995) Staurosporine-induced neuronal apoptosis. Exp Neurol 135:153–159
28. Cheung NS, Beart PM, Pascoe CJ, John CA, Bernard O (2000) Human Bcl-2 protects against AMPA receptor-mediated apoptosis. J Neurochem 74:1613–1620
29. Lim ML, Chen B, Beart PM, Nagley P (2006) Relative timing of redistribution of cytochrome *c* and Smac/DIABLO from mitochondria during apoptosis assessed by double immunocytochemistry on mammalian cells. Exp Cell Res 312:1174–1184
30. Desagher S, Martinou JC (2000) Mitochondria as the central control point of apoptosis. Trends Cell Biol 10:369–377
31. Waterhouse NJ, Goldstein JC, von Ahsen O, Schuler M, Newmeyer DD, Green DR (2001) Cytochrome c maintains mitochondrial transmembrane potential and ATP generation after outer mitochondrial membrane permeabilization during the apoptotic process. J Cell Biol 153:319–328
32. Houde C, Banks KG, Coulombe N, Rasper D, Grimm E, Roy S, Simpson EM, Nicholson DW (2004) Caspase-7 expanded function and intrinsic expression level underlies strain-specific brain phenotype of caspase-3-null mice. J Neurosci 24:9977–9984
33. Cheung EC, Joza N, Steenaart NA, McClellan KA, Neuspiel M, McNamara S, MacLaurin JG, Rippstein P, Park DS, Shore GC, McBride HM, Penninger JM, Slack RS (2006) Dissociating the dual roles of apoptosis-inducing factor in maintaining mitochondrial structure and apoptosis. Embo J 25:4061–4073
34. Saito A, Maier CM, Narasimhan P, Nishi T, Song YS, Yu F, Liu J, Lee YS, Nito C, Kamada H, Dodd RL, Hsieh LB, Hassid B, Kim EE, Gonzalez M, Chan PH (2005) Oxidative stress and neuronal death/survival signaling in cerebral ischemia. Mol Neurobiol 31:105–116
35. Nicholls DG (2008) Oxidative stress and energy crises in neuronal dysfunction. Ann N Y Acad Sci 1147:53–60
36. Dare E, Gorman AM, Ahlbom E, Gotz M, Momoi T, Ceccatelli S (2001) Apoptotic morphology does not always require caspase activity in rat cerebellar granule neurons. Neurotox Res 3:501–514
37. Valencia A, Moran J (2004) Reactive oxygen species induce different cell death mechanisms in cultured neurons. Free Radic Biol Med 36:1112–1125
38. Moore JD, Rothwell NJ, Gibson RM (2002) Involvement of caspases and calpains in cerebrocortical neuronal cell death is stimulus-dependent. Br J Pharmacol 135:1069–1077
39. Kroemer G, Galluzzi L, Vandenabeele P, Abrams J, Alnemri ES, Baehrecke EH, Blagosklonny MV, El-Deiry WS, Golstein P, Green DR, Hengartner M, Knight RA, Kumar S, Lipton SA, Malorni W, Nunez G, Peter ME, Tschopp J, Yuan J, Piacentini M, Zhivotovsky B, Melino G (2009) Classification of cell death: recommendations of the Nomenclature Committee on Cell Death 2009. Cell Death Differ 16:3–11
40. Galluzzi L, Kroemer G (2008) Necroptosis: a specialized pathway of programmed necrosis. Cell 135:1161–1163
41. Degterev A, Huang Z, Boyce M, Li Y, Jagtap P, Mizushima N, Cuny GD, Mitchison TJ, Moskowitz MA, Yuan J (2005) Chemical inhibitor of nonapoptotic cell death with therapeutic potential for ischemic brain injury. Nat Chem Biol 1:112–119
42. Degterev A, Hitomi J, Germscheid M, Ch'en IL, Korkina O, Teng X, Abbott D, Cuny GD, Yuan C, Wagner G, Hedrick SM, Gerber SA, Lugovskoy A, Yuan J (2008) Identification of RIP1 kinase as a specific cellular target of necrostatins. Nat Chem Biol 4:313–321
43. Xu X, Chua CC, Kong J, Kostrzewa RM, Kumaraguru U, Hamdy RC, Chua BH (2007) Necrostatin-1 protects against glutamate-induced glutathione depletion and caspase-independent cell death in HT-22 cells. J Neurochem 103:2004–2014
44. Zhang Z, Yang X, Zhang S, Ma X, Kong J (2007) BNIP3 upregulation and EndoG translocation in delayed neuronal death in stroke and in hypoxia. Stroke 38:1606–1613
45. Willaime S, Vanhoutte P, Caboche J, Lemaigre-Dubreuil Y, Mariani J, Brugg B (2001) Ceramide-induced apoptosis in cortical neurons is mediated by an increase in p38 phosphorylation and not by the decrease in ERK phosphorylation. Eur J Neurosci 13:2037–2046
46. Lakhani SA, Masud A, Kuida K, Porter GA Jr, Booth CJ, Mehal WZ, Inayat I, Flavell RA (2006) Caspases 3 and 7: key mediators of mitochondrial events of apoptosis. Science 311:847–851
47. Carmody RJ, Cotter TG (2000) Oxidative stress induces caspase-independent retinal apoptosis in vitro. Cell Death Differ 7:282–291
48. Haendeler J, Weiland U, Zeiher AM, Dimmeler S (1997) Effects of redox-related congeners of NO on apoptosis and caspase-3 activity. Nitric Oxide 1:282–293
49. Barbouti A, Amorgianiotis C, Kolettas E, Kanavaros P, Galaris D (2007) Hydrogen peroxide inhibits caspase-dependent apoptosis

by inactivating procaspase-9 in an iron-dependent manner. Free Radic Biol Med 43:1377–1387
50. Lee YJ, Shacter E (2000) Hydrogen peroxide inhibits activation, not activity, of cellular caspase-3 in vivo. Free Radic Biol Med 29:684–692
51. David KK, Sasaki M, Yu SW, Dawson TM, Dawson VL (2006) EndoG is dispensable in embryogenesis and apoptosis. Cell Death Differ 13:1147–1155
52. Cote J, Ruiz-Carrillo A (1993) Primers for mitochondrial DNA replication generated by endonuclease G. Science 261:765–769
53. Low RL (2003) Mitochondrial Endonuclease G function in apoptosis and mtDNA metabolism: a historical perspective. Mitochondrion 2:225–236
54. Ohsato T, Ishihara N, Muta T, Umeda S, Ikeda S, Mihara K, Hamasaki N, Kang D (2002) Mammalian mitochondrial endonuclease G. Digestion of R-loops and localization in intermembrane space. Eur J Biochem 269:5765–5770
55. Irvine RA, Adachi N, Shibata DK, Cassell GD, Yu K, Karanjawala ZE, Hsieh CL, Lieber MR (2005) Generation and characterization of endonuclease G null mice. Mol Cell Biol 25:294–302
56. Bahi N, Zhang J, Llovera M, Ballester M, Comella JX, Sanchis D (2006) Switch from caspase-dependent to caspase-independent death during heart development: essential role of endonuclease G in ischemia-induced DNA processing of differentiated cardiomyocytes. J Biol Chem 281:22943–22952
57. Nielsen M, Zimmer J, Diemer NH (2008) Endonuclease G expression in thalamic reticular nucleus after global cerebral ischemia. Exp Brain Res 190:81–89
58. Lee BI, Lee DJ, Cho KJ, Kim GW (2005) Early nuclear translocation of endonuclease G and subsequent DNA fragmentation after transient focal cerebral ischemia in mice. Neurosci Lett 386:23–27
59. Takano J, Tomioka M, Tsubuki S, Higuchi M, Iwata N, Itohara S, Maki M, Saido TC (2005) Calpain mediates excitotoxic DNA fragmentation via mitochondrial pathways in adult brains: evidence from calpastatin mutant mice. J Biol Chem 280:16175–16184
60. Hansen TM, Nagley P (2003) AIF: a multifunctional cog in the life and death machine. Sci STKE 2003:PE31
61. Susin SA, Lorenzo HK, Zamzami N, Marzo I, Snow BE, Brothers GM, Mangion J, Jacotot E, Costantini P, Loeffler M, Larochette N, Goodlett DR, Aebersold R, Siderovski DP, Penninger JM, Kroemer G (1999) Molecular characterization of mitochondrial apoptosis-inducing factor. Nature 397:441–446
62. Smith DJ, Ng H, Kluck RM, Nagley P (2008) The mitochondrial gateway to cell death. IUBMB Life 60:383–389
63. Boujrad H, Gubkina O, Robert N, Krantic S, Susin SA (2007) AIF-mediated programmed necrosis: a highly regulated way to die. Cell Cycle 6:2612–2619
64. Northington FJ, Zelaya ME, O'Riordan DP, Blomgren K, Flock DL, Hagberg H, Ferriero DM, Martin LJ (2007) Failure to complete apoptosis following neonatal hypoxia-ischemia manifests as "continuum" phenotype of cell death and occurs with multiple manifestations of mitochondrial dysfunction in rodent forebrain. Neuroscience 149:822–833
65. Degterev A, Yuan J (2008) Expansion and evolution of cell death programmes. Nat Rev Mol Cell Biol 9:378–390